Motor pattern generation is robust to neural network anatomical imbalance favoring inhibition but not excitation

Myriam Lauren de Graaf[1,2,3*], Luis Mochizuki[4], Frederik Thies[1], Heiko Wagner[1,2], and Charlotte Le Mouel[1]

[1] *Dept. of Movement Science, University of Münster, Horstmarer Landweg 62b, 48149 Münster, Germany*

[2] *Otto Creutzfeldt Center for Cognitive and Behavioral Neuroscience, University of Münster, Germany*

[3] *Center for Nonlinear Science (CeNoS), University of Münster, Corrensstraße 2, 48149, Münster, Germany*

[4] *School of Arts, Sciences and Humanities, University of São Paulo, Brazil*

[*] *Corresponding author: mdegraaf@uni-muenster.de*

Abstract

Animals display rich and coordinated motor patterns during walking and running. Previous modelling as well as experimental results suggest that the balance between excitation and inhibition in neural networks may be critical for generating such structured motor patterns. However, biological neural networks have an anatomical imbalance between excitatory and inhibitory neural populations. We explore the influence of such an anatomical imbalance on the ability of a reservoir computing artificial neural network to learn human locomotor patterns for slow walking, fast walking and running. We varied the numbers of neurons, connections percentages and connection strengths of excitatory and inhibitory populations. We showed that performance depended on the network anatomy. First, it deteriorated when the total number of neurons was too small or the total connection strength was too large. Second, performance was critically dependent on the balance between excitation and inhibition. Imbalance towards excitation caused a reduction in the richness of internal network dynamics, leading to a stereotypical motor output and poor overall performance. In contrast, rich internal dy-

namics and good overall performance were found when the network anatomy was either balanced or imbalanced towards inhibition. This suggests that motor pattern generation may be robust to increased inhibition but not increased excitation in neural networks.

1 Author summary

How does the anatomy of the nervous system allow the generation of the complex motor patterns observed during the movements of humans and other animals? We explore this question in a model of the spinal cord in which we vary the neural anatomy. We find that movement generation requires the neural network to have rich internal dynamics. Such rich internal dynamics emerge from the interaction between the excitatory and inhibitory neurons in the network. Strong inhibition causes fluctuations in the neural activity which allow rich motor patterns to be produced. However, strong excitation quenches these fluctuations and causes a reduction in the variability of motor patterns. When both excitation and inhibition are strong, the neural activity becomes chaotic, and dysfunctional, highly variable motor patterns are produced. We therefore predict that diseases of the nervous system which affect inhibitory and excitatory neurons differently will have a different signature in terms of motor patterns. Diseases causing increased excitation in neural circuits should lead to stereotypical motor behaviors, whereas diseases causing increased excitation and inhibition should lead to unstable motor patterns.

Keywords— EI balance, artificial neural networks, reservoir computing, inhibition, locomotion

2 Introduction

During walking and running, humans and other animals create rich and coordinate motor patterns, with muscle contractions by and large repeated in every step. This results in a rhythmic pattern of muscle contraction during locomotion. When walking faster or switching to running, not only does the rhythm accelerate, but the exact pattern of muscle contraction also changes, i.e. the amplitude of the contraction of each muscle changes, as well as its timing within the step cycle (Ivanenko et al., 2004, 2006; Lacquaniti et al., 2012). Neural systems able to produce various rhythms, called Central Pattern Generators, have been identified within the spinal cord (Delcomyn, 1980; IJspeert, 2008; Grillner, 1985).

The spinal cord is able to transform these basic rhythms into the rich and structured muscle contraction patterns required for locomotion at different speeds.

How the neural circuits within the spinal cord transform such simple rhythmic signals into structured motor commands may be understood with the framework of "reservoir computing". Simulation studies have shown that recurrent neural networks are able to produce complex, high-dimensional signals, even when the input signal it receives is very simple or absent (Funahashi & Nakamura, 1993). In reservoir computing (Verstraeten et al., 2007), such recurrent neural networks are used as a static reservoir, and only linear readouts of the network's activity are trained to reproduce a variety of target signals, without the need to adapt the internal connection weights in the network. For example, the reservoir activity can be read out to reproduce the trajectories of markers placed on the human body during walking and running (Sussillo & Abbott, 2009). Reservoir computing has been used to model how biological neural networks achieve a variety of tasks (Hinaut & Dominey, 2013; Boström, 2013; Wyffels & Schrauwen, 2009). It provides an interesting model as it captures three important properties of biological neural networks: (1) they are recurrent (i.e. the neural units are interconnected), (2) with sparse connections (i.e. there is a low probability for any two given neurons to be connected) and (3) random connection strengths (also called synaptic weights). The neurons themselves can be modelled with varying degrees of biological realism: Reservoir computing encompasses both *echo state networks*, which typically use simple firing-rate descriptions of neural activity (Jaeger, 2010), and *liquid state machines*, which implement spiking neurons (Maass et al., 2002).

Neural network function is thought to depend on a functional balance between excitation and inhibition. When balanced, the inhibitory and excitatory inputs to any neuron largely cancel each other out (Rubin et al., 2017). As a result, small fluctuations in the input to a neuron have a comparatively large effect on the neuron's output (Van Vreeswijk & Sompolinsky, 1996; Shadlen & Newsome, 1998; Amit & Brunel, 1997). This leads to a state of spontaneous chaotic activity (Van Vreeswijk & Sompolinsky, 1996), which is beneficial for reservoir computing, provided the chaos is not too large (Sussillo & Abbott, 2009). Within the reservoir computing framework, EI balance has been modelled with varying degrees of biological realism. *Echo state networks* typically do not have distinct excitatory and inhibitory neurons: the outgoing connection weights of individual neurons are most often drawn from a random distribu-

tion centered around zero (Sussillo & Abbott, 2009; Boström, 2013; Jaeger, 2010). As a result, any given neuron exerts both excitatory and inhibitory influences. In these networks, functional EI balance is thus imposed in a non-biological manner, through a strict anatomical balance between excitatory and inhibitory connections.

Biological networks, on the other hand, consist of distinct excitatory and inhibitory neural populations. The outputs of any given neuron are either all excitatory or all inhibitory (Eccles, 1976), a phenomenon known as Dale's law. Activity within the network depends on a functional balance between excitation and inhibition (Zhou & Yu, 2018). Anatomically, however, the excitatory and inhibitory populations are not equal. For instance, there are typically more excitatory than inhibitory neurons: inhibitory neurons make up only 30 to 45 % of the neurons in laminae I to III of the rat spinal cord (Todd & Sullivan, 1990), and only around 20% of the neurons in the mammalian cerebral cortex (Marom & Shahaf, 2002; Sahara et al., 2012; Marín, 2012; Wonders & Anderson, 2006; Meinecke & Peters, 1987). Moreover, excitatory and inhibitory connection probabilities are not identical. For example, in the cortex, only one in fifteen inputs to a given neuron is inhibitory (Megías et al., 2001; Peters, 2002). So, while the proper functioning of biological neural networks depends on the ratio of excitation to inhibition, this is a functional balance resulting from network dynamics, rather than the result of a strict anatomical balance.

The purpose of our study is to explore how anatomical differences in excitatory and inhibitory populations influence neural network dynamics and performance. We modified an echo state neural network proposed by Sussillo & Abbott (2009) such that: (1) synaptic weights from any given neuron were either all positive or all negative, and (2) the firing rates of all neurons were constrained to be positive. As a result, individual neurons in the network could be considered either excitatory or inhibitory. We tested whether the dynamics of the network are affected by the ratio of excitatory to inhibitory neuron number, connection percentage and connections strength. We showed that reservoir computing is robust to increased inhibition, but not to increased excitation.

3 Results

Echo state networks with distinct excitatory and inhibitory neural populations were trained to reproduce three locomotor signals corresponding to slow walking, fast walking, and running, using the FORCE

algorithm (Sussillo & Abbott, 2009). We varied the number of neurons (Figure 1A&B), the connection strength (Figure 1C&D), and the connection percentage (Figure 1E&F) of the excitatory and inhibitory neurons populations separately. The connection percentage and connection strength were varied for 5 different ratios of excitatory neuron number (N_E) to inhibitory neuron number (N_I). Results for the non equal excitatory and inhibitory neuron numbers can be found in Figures S.2 and S.3. After learning, the networks were tested on their ability to generate the aforementioned locomotor patterns when receiving a sinusoidal input at the corresponding stride frequency. The network performance was expressed as the percentage of gait cycles that were successfully reproduced, i.e. with a root mean square error (RMSE) smaller than 0.05. The richness of the internal network dynamics was quantified as the number of principal components needed to explain 99% of temporal variance in the neuron firing rates, referred to as Network Principal Components (NPCs) from now on.

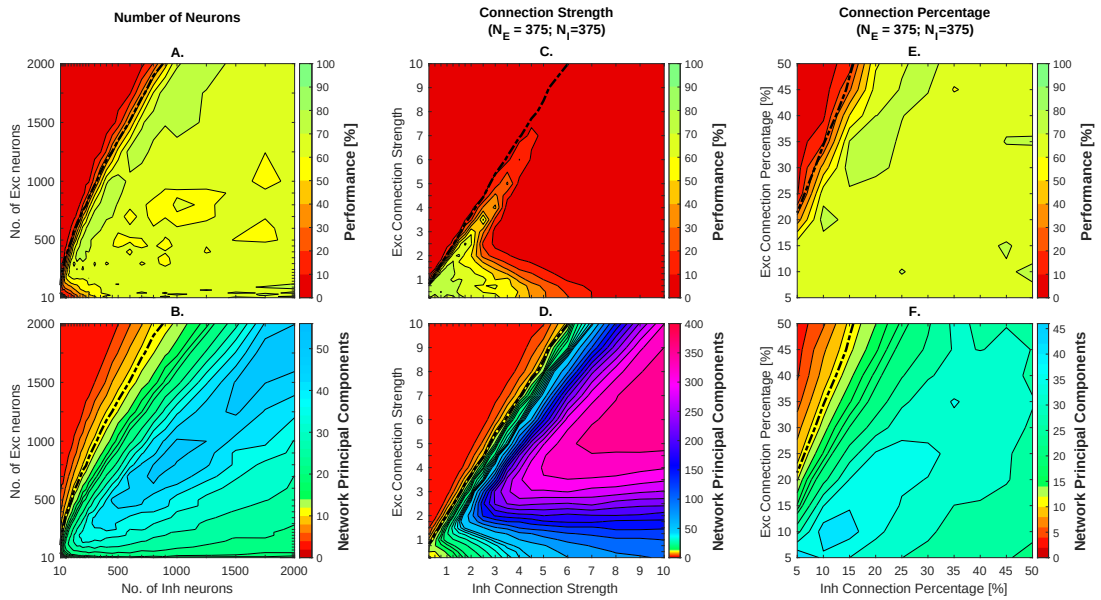

Figure 1 – Influence of network anatomy on performance and internal network dynamics. *Network performance (top row) and number of Network Principal Components (bottom row) as a function of* ***(A. & B.)*** *neuron number (with $p_E = p_I = 0.1$ and $g_E = g_I = 1.5$),* ***(C. & D.)*** *connection percentage (with $N_E = N_I = 375$ and $g_E = g_I = 1.5$), and* ***(E. & F.)*** *connection strength (with $N_E = N_I = 375$ and $p_E = p_I = 0.1$). Overlayed in all panels as a thick dashed-dotted black line is the contour line indicating 11 NPCS, which corresponds to the number of principal components needed to explain 99% of variance in the target data.*

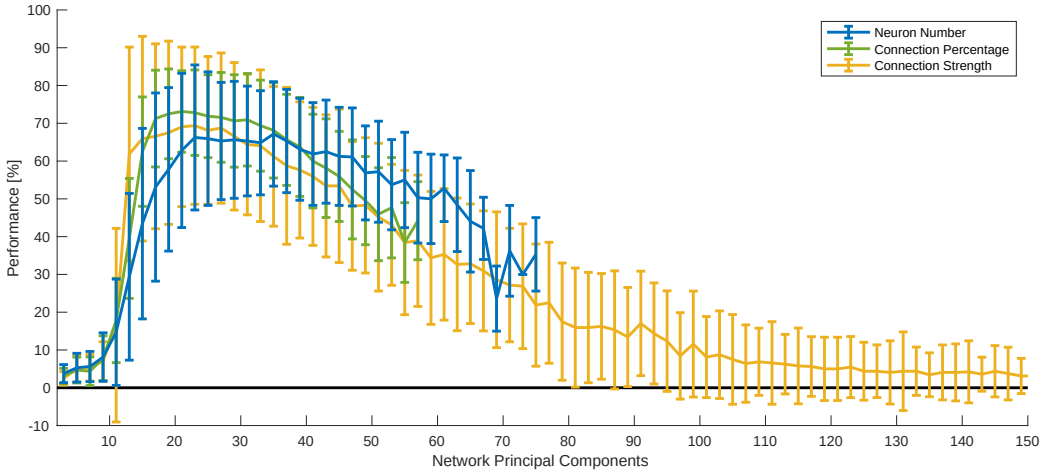

Figure 2 – Performance depends on the internal network dynamics. *Performance as a function of the number of NPCs when varying the Neuron Numbers (blue), Connection Percentages (green) and Connection Strengths (yellow).*

3.1 The dependence of performance on network anatomy is mediated by the internal network dynamics

We found a strong correspondence between network performance and the number of NPCs. Varying either the number of neurons (blue in Figure 2), the connection percentages (green in Figure 2), or the connection strengths (yellow in Figure 2) led to networks with a large variety in the number of NPCs (ranging from 2 to 410). Networks with less than 11 NPCs failed consistently (average performance of 4.4%), with performance rising sharply for networks with at least 11 NPCs. This transition corresponds to the number of principal components necessary to account for 99% of the variance in the target locomotor patterns. In addition, performance deteriorates for networks with more than 40 NPCs, indicating that these networks are too chaotic to support learning.

3.2 Networks with low neuron numbers have low performance because their internal dynamics are too poor

Across the three tested parameters, we identified three distinct regions where networks failed to reproduce locomotor patterns. First, networks were unsuccessful if the total neuron number ($N = N_E + N_I$, where N_E and N_I are the numbers of excitatory and inhibitory neurons) was too low (below 300, see Figure 1A, bottom left corner, & Figure 3A). These networks had a low number of NPCs (Figure 1.B, bottom

left corner, & Figure 3B). An expanded view of the low neuron number region is presented in Supplementary Figure S.1. Increasing the neuron number up to 300 neurons, there is a steady increase in both NPCs (Figure 3B) and performance (Figure 3A). This suggests that, for networks with too few neurons, the internal network dynamics are not rich enough to produce locomotor patterns. Therefore, networks with less than 300 neurons were discarded from further analysis.

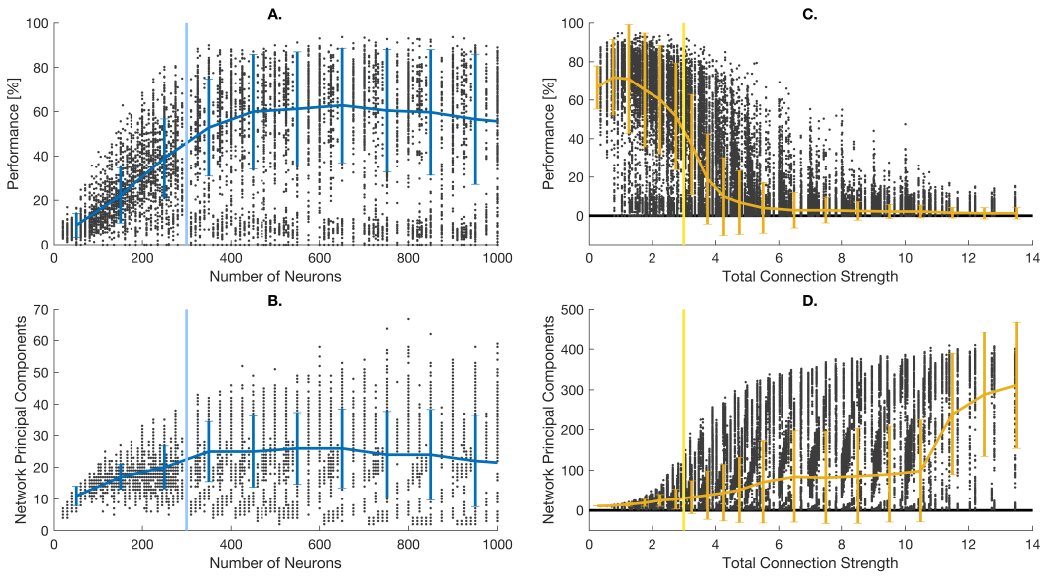

Figure 3 – Low performance for networks with a very small neuron number or a very high connection strength is mediated by the number of NPCs. *Networks with less than 300 neurons (vertical light blue line) have low performance (**A.**) and a low number of Network Principal Components (**B.**) Networks with total connection strength larger than 3 (vertical yellow line) have low performance (**C.**) and a very high number of Network Principal Components (**D.**). For all panels, each dot represents one network. For connection strength, results for all five $N_E : N_I$ ratios are shown. The dark blue and yellow bars indicate the median and standard deviation per bin.*

3.3 Networks with large connection strengths have low performance because their dynamics are too chaotic

Second, networks were unsuccessful if the total connection strength ($g = \sqrt{g_E^2 + g_I^2}$, where g_E is the connection strength of the excitatory and g_I of the inhibitory population) of the networks was too high (above 3, Figure 1C, right side red zone, and Figure 3C). These networks had a very large number of NPCs (Figure 1D, right side blue to pink zone and Figure 3D). As previously described, while performance initially improves when the number of NPCs rises, it decreases again when the number of principal components becomes too high (Figure 2). The latter occurs when the total connection strength of the network is too high: there is a dramatic increase in the number of NPCs for networks with in-

creasing total connection strength (Figure 3D). As a result, the average network performance decreases as connection strength increases beyond $g \approx 1$, reaching a median performance of about 50% for $g = 3$ and then dropping sharply (Figure 3C). We thus limit our analyses to networks with a total connection strength of 3 or lower.

3.4 Performance is robust to anatomical imbalance favoring inhibition but not excitation

Finally, networks were unsuccessful when excitation was stronger than inhibition (Figure 1A,C,E, top left red triangles). As derived in the Methods (Equation 3), the average recurrent input to a neuron (I_{rec}) depends on the average firing rate r and on the excitatory and inhibitory neuron numbers (N_E and N_I), connection percentages (p_E and p_I) and connection strengths (g_E and g_I). We defined the imbalance between excitation and inhibition in the network as the ratio between the average recurrent input and the average firing rate (Methods Equation 4):

$$Imbalance = \sqrt{\frac{2}{\pi}}(g_E\sqrt{p_E N_E} - g_I\sqrt{p_I N_I})$$

Balanced networks (Imbalance = 0) had a good overall performance (Figure 4A). However, performance deteriorated when excitation was markedly stronger than inhibition (Figure 4A, Imbalance > 3), whether in terms of connection percentage (Figure 4A, in green), neuron number (Figure 4A, in blue) or connection strength (Figure 4A, in yellow). This drop in performance corresponded to a sharp decrease in the number of NPCs (Figure 4B). Indeed, when a network is strongly imbalanced towards excitation, the mean input received by the neurons is large and positive (Figure 4C). Therefore, the average neural firing rate saturates to its maximum value of one (Figure 4D) and the variance in firing rate drops close to zero (Figure 4E). As a result, networks whose internal structure is too far imbalanced towards excitation are not able to produce locomotor patterns (Figure 4A).

In contrast, network performance was very robust to an imbalance favoring inhibition. In networks imbalanced towards inhibition (Imbalance < 0), the mean input received by the neurons is negative (Figure 4C). The neurons' firing rate is then driven purely by fluctuations in the recurrent input. This

fluctuation-driven regime prevents the firing rates from saturating to their minimum value of zero (Figure 4D). Therefore, individual neurons maintain some temporal variability in their firing rate (Figure 4E), enough for proper network variability (Figure 4B) to enable the network to produce the locomotor patterns (Figure 4A).

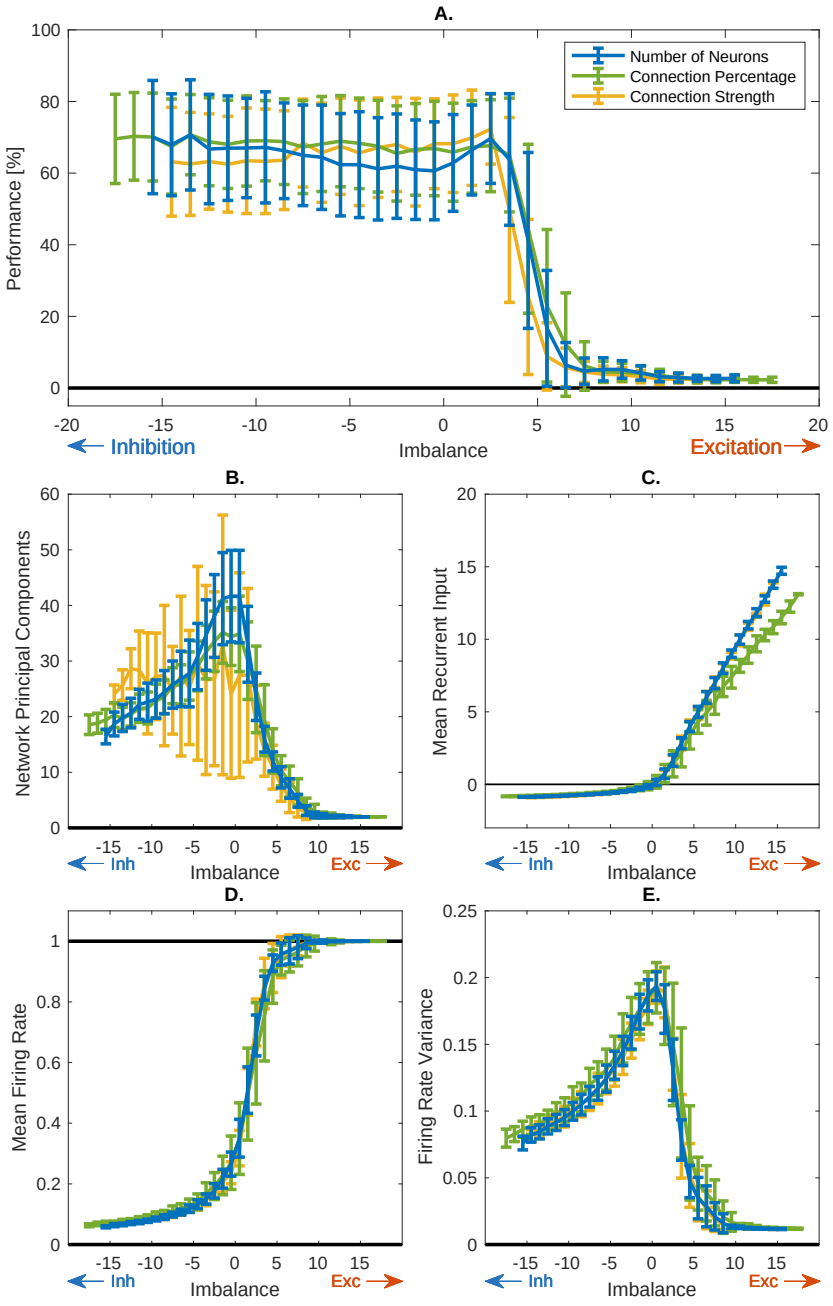

Figure 4 – Network performance is robust to inhibitory, but not excitatory, imbalance. *Network performance (**A**), mean recurrent input (**B**), firing rate (**C**), firing rate variance (**D**), and network principal components (**E**) as a function of imbalance. In each plot, the mean and standard deviation per bin are shown for: Neuron Number (blue), with N_E and N_I ranging from 10 to 2000 in increasing steps, $p_E = p_I = 0.1$ and $g_E = g_I = 1.5$; Connection Percentage (green), with p_E and p_I ranging from 0.05 to 0.5 in steps of 0.05, and $g_E = g_I = 1.5$; Connection Strength (yellow), with g_E and g_I ranging from 0.1 to 10 in increasing steps and $p_E = p_I = 0.1$. For connection percentage and strength, neuron numbers were varied with total network size $N_E + N_I$ equal to 750: $N_E : N_I$ = 600:150, 500:250, 375:375, 250:500 and 150:600.*

4 Discussion

The aim of this study was to model the influence of EI balance on the ability of an artificial neural network to reproduce the locomotor patterns observed during human walking and running. We implemented a classical network architecture used for reservoir computing (Sussillo & Abbott, 2009), and modified the network anatomy so that it contains distinct excitatory and inhibitory pools. We then varied the ratios of excitatory to inhibitory neuron numbers, connection percentages and connection strengths. Altogether, network performance seems to rely on the network dynamics having both sufficient richness (equal or more PCs than in the target output) and sufficient structure (in this case, less than 40 NPS). Our findings show that rich internal dynamics are maintained in networks imbalanced towards inhibition, but that this variability is quenched in networks imbalanced towards excitation. Network performance is therefore robust to increased inhibition, but not to increased excitation.

4.1 Performance requires rich but structured neural network dynamics

We found that performance was well explained by the variability in the internal network dynamics (see Figure 2). We quantified the richness and structure of the internal network dynamics by measuring the number of principal components accounting for 99% of the variability in neuron firing rates ("network principal components" or NPCs). Performance decreased when the number of NPCs decreased. Indeed, the network's task is to reproduce locomotor patterns through a linear readout of the internal dynamics. These target locomotor patterns require 11 principal components to account for 99% of their variance. Therefore, in principle, networks with fewer than 11 NPCs should not be able to successfully reproduce all patterns. In practice, we found that network performance started to drop when the number of NPCs decreased below 20. Moreover, performance decreased for networks with too many NPCs, suggesting that the network dynamics become too chaotic for structured motor patterns to be read out.

4.2 Network anatomy determines network dynamics and therefore performance

The internal network dynamics, and therefore the network performance, depended on the network architecture (total neuron number and total connection strength) and the overall anatomical balance be-

tween excitation and inhibition in the network (described by Equation 4).

When varying the total neuron number, we found a decrease in the number of NPCs (Figure 3B) and performance (Figure 3A) for networks with less than 300 neurons. This suggests that reservoir computing might not be an appropriate model for the generation of motor patterns in small neural networks, such as the crab stomatogastric ganglion, which has only ~30 neurons (Selverston et al., 1976). Reservoir computing has, however, successfully been used to model the function of mammalian cortical circuits (Maass et al., 2002; Enel et al., 2016; Cazin et al., 2019; Dominey, 2021) and we suggest it may also be used to model the function of the vertebrate spinal cord, which contains a few hundred million neurons in humans.

When varying the total connection strength, we found a dramatic increase in the number of NPCs (Figure 3D) and a corresponding decrease in performance (Figure 3C) for networks with large total connection strengths. This confirms previous simulation results which show that large connection strengths lead to a decrease in reservoir computing performance (Sussillo & Abbott, 2009; Lukoševičius, 2012).

When varying the anatomical balance between excitation and inhibition, we found that networks were successful in two specific situations: (1) when excitation and inhibition in the network were balanced (Figure 4A, Imbalance = 0), or (2) if networks had an overall anatomical imbalance favoring inhibition (Figure 4A, negative Imbalance).

4.3 Overall anatomical balance can be achieved despite inequalities in individual anatomical parameters

In the case of an overall anatomical balance between excitation and inhibition, the two opposing input currents to any given neuron cancelled each other out on average. Such states of relative functional EI-balance have been observed experimentally in numerous regions of the mammalian cortex (Herstel & Wierenga, 2021; Isaacson & Scanziani, 2011; Wehr & Zador, 2003; Okun & Lampl, 2008, 2009; Atallah & Scanziani, 2009). Moreover, simulation results indicate that such functional EI-balance may be beneficial for a variety of neural network functions, such as the ability to respond quickly to changing inputs (Tsodyks & Sejnowski, 1995; Van Vreeswijk & Sompolinsky, 1996; van Vreeswijk & Sompolinsky, 1998) and noise robustness (Rubin et al., 2017). It is, however, not known how this functional EI-balance

arises from the network anatomy.

In biological neural networks, the anatomical characteristics of excitatory and inhibitory neurons do not follow a 1-to-1 ratio. For example, in the mammalian cortex, there seems to be an approximately 4-to-1 ratio in both excitatory to inhibitory neuron numbers (Marom & Shahaf, 2002; Sahara et al., 2012; Marín, 2012; Wonders & Anderson, 2006; Meinecke & Peters, 1987) and connection percentages (Megías et al., 2001; Peters, 2002). Our results show that the net current to the neurons can still be balanced, even if these individual anatomical parameters are not balanced.

In our model, we calculated the net average current from each of the two neuron pools (excitatory and inhibitory), and found that this scales with the pool's firing rate multiplied by an overall weight that depends on the pool's anatomical parameters (Equation 3). This weight scales linearly with the connection strengths, but with the square root of the neuron number and connection percentage. This suggests that the inequalities in the number of neurons and connection percentage can be compensated for by an approximate 1-to-4 ratio in excitatory to inhibitory connections strengths (provided the total connection strength does not become too large). There is indeed experimental evidence suggesting that connection strengths may be larger for inhibitory than excitatory neurons in the mammalian cortex, as they synapse closer to the axon somata (Beaulieu et al., 1992; Peters, 2002) thereby increasing their effectiveness relative to the excitatory neurons (Chen et al., 2012; Markram et al., 2004).

We also explored networks with a net anatomical imbalance, resulting in a functional imbalance in the average recurrent input to the neurons (Figure 4C), and showed that this did not necessarily lead to a decrease in performance (Figure 4A).

4.4 Good performance is maintained when anatomical imbalance favors inhibition

While biological networks seem to operate close to a state of functional EI-balance globally, the exact balance between excitatory and inhibitory seems to vary depending on, e.g., sensory stimulation and the circadian rhythm (Adesnik, 2017; Bridi et al., 2020; Tatti et al., 2017), suggesting that strict functional balance is not necessary for network performance.

Experimental manipulations of the EI-balance suggest that network function is robust to imbalance

favoring inhibition, but not to imbalance favoring excitation. Both increased excitation and decreased inhibition in the brain have been found to play a role in disorders such as epilepsy (Dichter & Ayala, 1987; Dudek & Sutula, 2007), autism (Casanova et al., 2003; Rubenstein, 2010; Rubenstein & Merzenich, 2003; Markicevic et al., 2020) and schizophrenia (Yizhar et al., 2011; Murray et al., 2014). In the spinal cord, disinhibition has been shown to lead to allodynia (Lee et al., 2019; Yaksh, 1989). In the mouse prefrontal cortex, information processing is impaired when excitation is increased but not when inhibition is increased Yizhar et al. (2011). In contrast, there is much more limited experimental evidence for impaired network function as a result of increased inhibition (but see for example Blundell et al. (2010) and Tabuchi et al. (2007) who show that increased inhibition due to genetic deletion can lead to autism-like behavior in mouse models). It is however not known why biological neural network function is robust to increased inhibition but not excitation.

In our model, we explored the influence of functional imbalance on network performance, by studying networks with an overall anatomical imbalance between excitation and inhibition (as described by Equation 4). We varied the anatomical ratios in neuron number, connection percentage and connection strength to achieve different states of overall anatomical imbalance between excitatory and inhibitory input currents. Confirming the experimental findings described in the previous paragraph, our modelling results show that network performance is highly robust to an anatomical imbalance favoring inhibition (Figure 4A, negative Imbalance). This leads to a nearly balanced functional state, in which inhibitory currents are only slightly larger than excitatory currents (Figure 4C, negative Imbalance). In contrast, there is a strong deterioration of performance for networks with an anatomical imbalance favoring excitation (Figure 4A, positive Imbalance). This leads to a highly unbalanced functional state, in which excitatory currents are much larger than inhibitory currents (Figure 4C, positive Imbalance). As a result, neural firing rates saturated to their maximal values (Figure 4D, positive Imbalance), resulting in reduction in firing rate variability (Figure 4E, positive Imbalance).

4.5 Reduced locomotor complexity as a signature of excitatory imbalance

Interestingly, we identified a particular signature of excitatory imbalance in terms of the output locomotor patterns. The muscle activation patterns observed during human locomotion typically vary within a

subspace whose dimensionality is smaller than the number of recorded muscles (Ivanenko et al., 2004; Neptune et al., 2009; Clark et al., 2010; Dominici et al., 2011; Chvatal & Ting, 2012). For example, in our study, we found that 11 principal components account for 99% of the variance in muscle activations observed during slow walking, fast walking and running. When we modified the neural network anatomy to increase excitation, this resulted in a reduction in the variability of the internal network dynamics (reduction in NPCs for positive Imbalance,Figure 4B), which led to a reduction in the variability of the output motor patterns Figure S.4. Our modelling results therefore suggest that a dysfunctional reduction in motor variability (characterized by a disappearance of motor synergies) would be a signature of increased excitation or decreased inhibition in neural motor circuits.

5 Methods

All data analysis described in the following sections was performed in Matlab (R2020a).

5.1 Reservoir Computing Neural network with asymmetric excitatory and inhibitory populations

5.1.1 Network Dynamics

The reservoir networks consist of an excitatory population E with neuron number N_E and an inhibitory population I with neuron number N_I. Any given neuron i receives an external input, output feedback and recurrent input. The external input is $J_i^{In} \cdot S$, where S is the sinusoidal input signal ranging from 0 to 2 at the target stride frequency (Figure 5, bottom left), and J_i^{In} are the input weights drawn from a Gaussian distribution with zero mean and unit variance. The output feedback is $J_i^{Fb} Y$, where Y is the output of the network (Figure 5, bottom right) and the feedback weights J_i^{Fb} are drawn from a uniform distribution between -1 and 1. The recurrent input can be split into an excitatory ($J_i^E r^E$) and inhibitory ($J_i^I r^I$) component, where r_E and r_I are the firing rate of the two populations. The connection weights J_{ij}^E from any excitatory neuron j to any neuron i have a probability p_E of being non-zero. For non-zero weights, the value is the absolute value of a variable drawn from a Gaussian distribution of mean zero and variance $g_E/(p_E N_E)$, where g_E will be referred to as the excitatory connection strength. In-

hibitory weights J^I_{ij} have a probability p_I of being non-zero. If non-zero, their value is the negative of the absolute value of a Gaussian random variable with mean zero and variance $g_I/(p_I N_I)$, with g_I the inhibitory connection strength. Note that in the original network proposed by Sussillo & Abbott (2009), all recurrent weights are drawn from a Gaussian distribution of mean zero and variance $g/(pN)$, therefore a given neuron can have both positive and negative output weights. In our network, the total input received by a given neuron i is:

$$I_i = J^{In}_i S + J^{Fb}_i Y + \sum_{j=1}^{N_E} J^E_{ij} r^E_j - \sum_{j=1}^{N_I} J^I_{ij} r^I_j \tag{1}$$

The internal state q_i of neuron i is initialized randomly, drawn from the standard normal distribution, and follows the dynamics:

$$\tau \frac{d}{dt} q_i = -q_i + I_i \tag{2}$$

with time constant $\tau = 0.01$. The differential equation was solved numerically using Euler-forward integration for each time step ($\Delta t = 0.005s$) to get the new neuron activation. The firing rate is $\tanh(q_i)$ if q_i is positive, and zero otherwise. In the original network proposed by Sussillo & Abbott (2009), the firing rate is $\tanh(q_i)$ and can be positive or negative depending on the sign of q_i.

5.1.2 Average input

Averaging across neurons, the mean external input and output feedback are both zero, as the weights are centered around a zero mean. In the original network proposed by Sussillo & Abbott (2009), the recurrent weights are also symmetrically distributed around zero. As a result, the net recurrent input received by neurons in the Sussillo & Abbott (2009) network is on average zero, independent of total neuron number, connection percentage or connection strength. In our networks, however, each neuron receives on average $p_E \cdot N_E$ non-zero excitatory weights, each with average value $g_E\sqrt{2/(\pi p_E N_E)}$, and $p_I N_I$ non-zero inhibitory weights, each with average value $-g_I\sqrt{2/(\pi p_I N_I)}$. Since the excitatory and inhibitory neurons receive inputs with the same weights, the average firing rates of the excitatory and inhibitory populations are the same, written here as r. The resulting average recurrent input to a neuron (I_{rec}) is, therefore:

$$I_{rec} = r\sqrt{\frac{2}{\pi}}(g_E\sqrt{p_E N_E} - g_I\sqrt{p_I N_I}) \tag{3}$$

We defined the imbalance between excitation and inhibition in the network as the ratio between the average recurrent input and the average firing rate:

$$Imbalance = \sqrt{\frac{2}{\pi}}(g_E\sqrt{p_E N_E} - g_I\sqrt{p_I N_I}) \tag{4}$$

then,

$$I_{rec} = r \cdot Imbalance \tag{5}$$

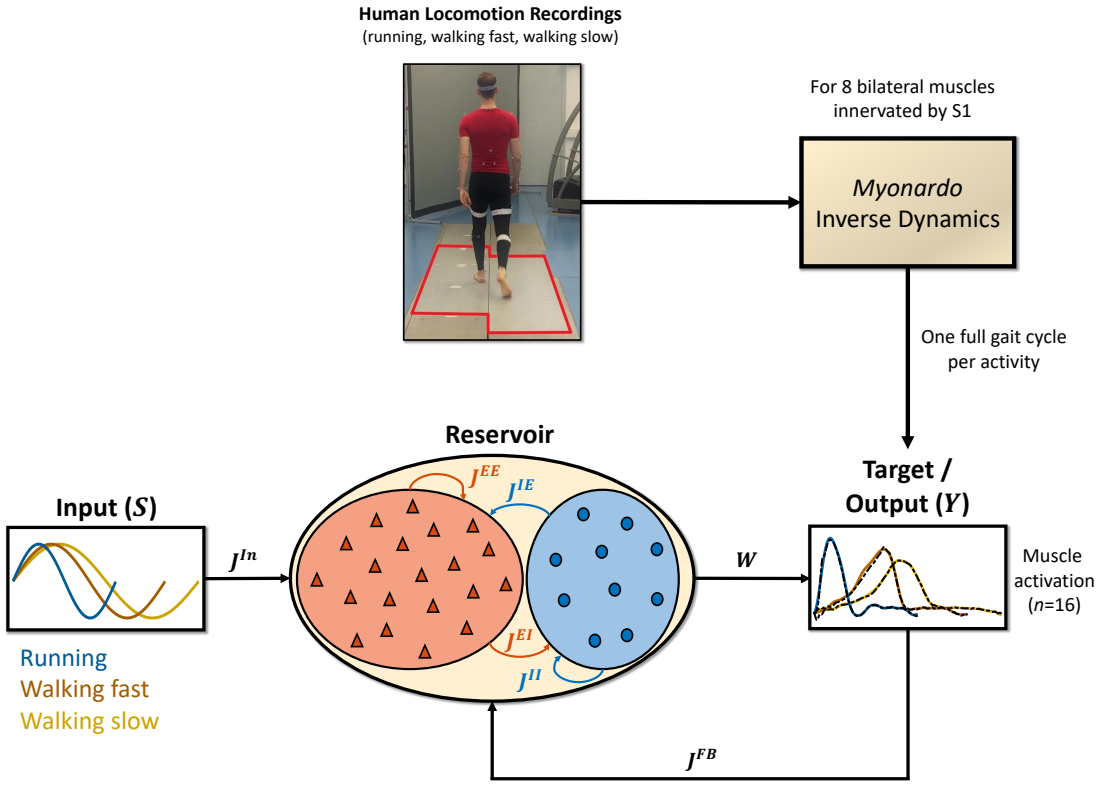

Figure 5 – Schematic overview of methods. *Human locomotor signals were recorded from one subject during walking slowly, walking faster and running (top middle). Ground reaction forces were recorded using six Kistler Force Platforms (outlined in red) and kinematics were recorded using a Qualisys measuring system. The recorded kinetics and kinematics were the input to the inverse dynamics calculations (top right), which provided the required muscle activation for 8 bilateral muscles. These muscle activations were used as the (16-dimensional) target output of the neural network (bottom right). The neural network (bottom middle) consists of two connected excitatory (red, triangles) and inhibitory (blue, circles) populations. In the network, blue lines denote inhibitory connections, while red lines denote excitatory connections. The input to the network (bottom left) was a sinusoid with a frequency corresponding to the gait frequency for each activity: running (blue), fast walking (brown) and slow walking (yellow).*

5.1.3 Network Parameters

Various ratios of excitation to inhibition were tested by varying the three different parameters that influence the excitatory to inhibitory (im)balance. First, the number of neurons was increased independently

for both pools from 10 to 2000 (from 10 to 50 in steps of 10, from 75 to 250 in steps of 25, from 300 to 500 in steps of 50, from 600 to 1000 in steps of 1000, and from 1250 to 2000 in steps of 250). Connection percentage was set constant at $p_E = p_I = 0.1$, corresponding to connection ratios found in *ex vivo* neural networks (Marom & Shahaf, 2002), and connection strength at $g_E = g_I = 1.5$, as this produced good network performance in Sussillo & Abbott (2009). Second, the connection percentages p_E and p_I were independently varied from $p = 0.05$ to 0.5 in steps of 0.05, for the inhibitory and excitatory populations independently. The effect of varying connection percentage was investigated for networks with a total neuron number of $N = 750$ and neuron ratio varying from $4:1$ to $1:4$, namely: N_E:N_I = 600:150, 500:250, 375:375, 250:500 and 150:600. Finally, the connection strengths g_E and g_I were independently varied from 0.1 to 10 in increasing steps (from 0.25 to 2 in steps of 0.25, from 2.5 to 5 in steps of 0.5, and from 6 to 10 in steps of 1). Again, the tests were performed for networks with several N_E:N_I ratios (600:150, 500:250, 375:375, 250:500 and 150:600) all with total size $N = 750$. The connection percentage was set constant at $p_E = p_I = 0.1$. For each set of parameters, 20 networks were randomly generated with the corresponding internal structure. Figure 1 and Figures S.1 to S.3 show the performance and NPCs averaged across these 20 networks, whereas in Figure 3 each network is shown as an individual dot.

5.2 Target signals

5.2.1 Experimental recording of human locomotion

Kinematics and ground reaction forces were recorded for three different locomotor activities: walking at two different (self-chosen) speeds and running. Kinetics were recorded using six Kistler force platforms (Type 9287CA, 90×60 cm, Kistler Instrumente AG, Winterthur, Switzerland - outlined in red in the photo in Figure 5). Whole-body kinematics were recorded at 200 Hz (Qualisys, Göteborg, Sweden) using a modified Plug-In Gait marker set (Vicon Motion Systems Ltd, Oxford, UK). A single participant (male, 26 years old, 1.96m tall and weighing 86kg) walked and ran across the length of the force-plates. This data was obtained as part of another experiment that has been approved by the local ethics committee of the Department of Sports Science and Psychology of the University of Münster (#2019-10-RD). The participant signed the informed consent form.

5.2.2 Target spinal pattern building blocks from inverse dynamics

Muscle activations were calculated from the recorded kinetics and kinematics using the inverse dynamics function of the musculo-skeletal model *Myonardo*®. For more information on the musculo-skeletal model and the performed calculations, see Appendix A. From the model output, we selected the bilateral muscles that are innervated by the S1 spinal segment: (*m. flexor hallucis longus*, *m. gastrocenemius*, *m. gluteus maximus*, *m. gluteus medius*, *m. gluteus minimus*, *m. piriformis*, *m. semitendinosus*, and *m. tensor fasciae latae*) resulting in 16 target spinal signals.

For each of the three activities, a single stride from right heel strike to the following right heel strike was selected as a building block, from which the full target signals were created in a later step. The heel strikes were detected by finding the lowest point of the right heel marker, as recorded by the Qualisys system. The activity of each muscle was normalized by its maximal activity across the 3 locomotor patterns.

5.2.3 Signal creation

The training and test signals were then assembled from the single-stride building blocks. To train the networks, input and output signals were created where each of the three activities was repeated for five consecutive strides. To test the networks, signals consisting of 20 gait cycles were created, with the activity of each cycle chosen randomly, but with each activity represented for at least one cycle. The same set of signals was used for all networks within one trial. The transitions between two consecutive cycles were smoothed by leaving one-sample gaps between the different activities that were linearly interpolated. The entire signal was filtered using a 20 Hz low-pass bi-directional Butterworth filter (2^{nd} order) to further smooth the signal. Finally, the first and last 50 samples were cut from all signals to remove any unwanted filter artifacts. An example of a full test signal for one muscle can be found in Figure S.4C.

5.3 Training and testing the Networks

We applied the FORCE learning algorithm (Sussillo & Abbott, 2009) to train the networks and assessed the ability of reservoir networks with asymmetrical inhibitory and excitatory populations to produce a given target spinal pattern when receiving a sinusoidal input whose frequency matches the target stride

frequency (corresponding to either to slow walking, fast walking or running). For each combination of network parameters, we tested 20 different recurrent networks, each with a random instantiation of the connection weights.

5.3.1 FORCE Learning

The output weights of the networks were trained using the FORCE method (Sussillo & Abbott, 2009), a technique that uses a recursive least squares algorithm (Haykin, 2014). Unlike the internal connection weights, the output weights of the network were not restricted to be positive during training and can be either negative or positive. All networks were trained over 15 consecutive repetitions. See Appendix B for a more detailed description of FORCE learning.

5.3.2 Outcome parameters

The performance of each network was quantified as the percentage of successfully reproduced cycles. First, the root-mean-square error (RMSE) between the predicted (dashed black lines, Figure 6) and target (colored lines, Figure 6) output was calculated for each muscle and each of the 20 gait cycles in the test signal. This error followed a roughly bimodal distribution (Figure S.4B). The threshold for success was set at RMSE = 0.05, chosen to fall between the two first peaks of this distribution (solid black line Figure S.4B). Using this criterion, the pattern produced by each muscle during each cycle was either classified as a success ($RMSE < 0.05$, shaded in green in Figure 6 and Figure S.4C) or a failure ($RMSE > 0.05$, shaded in red in Figure 6 and Figure S.4C). The richness of the internal network dynamics was quantified as the number of principal components that are necessary to account for 99% of the temporal variance in the neuron firing rates.

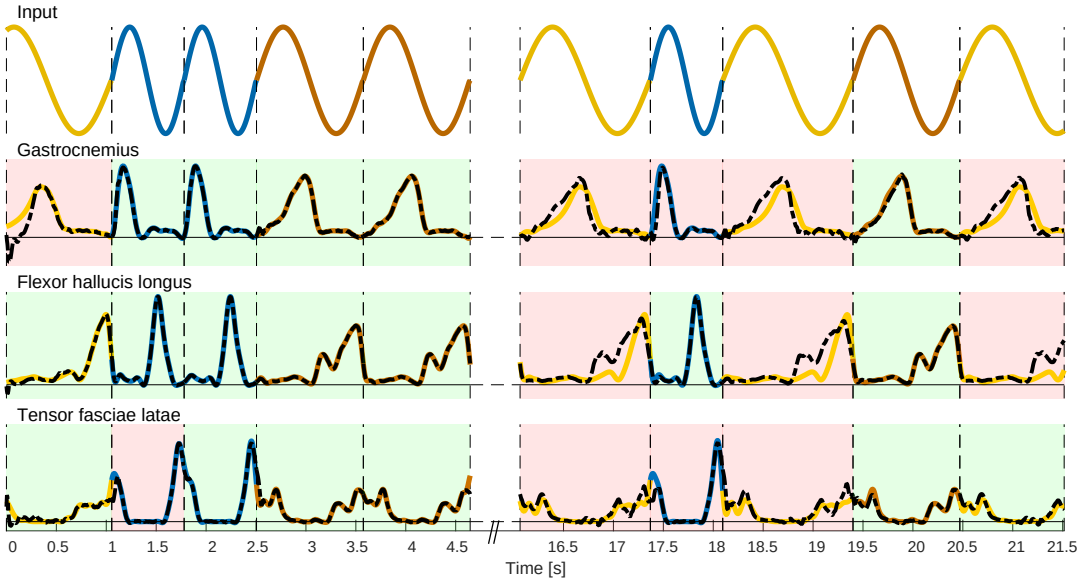

Figure 6 – Performance calculation in an example output. *The network is tested on its ability to reproduce the motor patterns of randomly interleaved gait cycles. The input to the network (top row) and target motor outputs of three example muscles (bottom rows) are shown in yellow for slow walking, brown for fast walking and blue for running. The actual network output is indicated as a dashed black line (bottom rows). The transitions between cycles are indicated as dashed vertical black lines. For each cycle and muscle, if the root mean square difference between the target and the motor output is less than 0.05, this is classified as a success, indicated as a green background. Otherwise, it is classified as a failure, indicated as a red background. The performance of the network is the percentage of successful cycles over all 20 test cycles and 16 muscles.*

Acknowledgements

Analyses were run on the high performance computer PALMA of the University of Münster. We thank

Kim Boström for his help with the Myonardo model.

References

Adesnik, H. (2017, aug). Synaptic Mechanisms of Feature Coding in the Visual Cortex of Awake Mice. *Neuron*, *95*(5), 1147–1159.e4. doi: 10.1016/J.NEURON.2017.08.014

Amit, D. J., & Brunel, N. (1997). Model of global spontaneous activity and local structured activity during delay periods in the cerebral cortex. *Cerebral Cortex*, *7*(3), 237–252. doi: 10.1093/cercor/7.3.237

Atallah, B. V., & Scanziani, M. (2009, may). Instantaneous Modulation of Gamma Oscillation Frequency by Balancing Excitation with Inhibition. *Neuron*, *62*(4), 566–577. doi: 10.1016/j.neuron.2009.04.027

Beaulieu, C., Kisvarday, Z., Somogyi, P., Cynader, M., & Cowey, A. (1992). Quantitative Distribution of GABA-immunopositive and-immunonegative Neurons and Synapses in the Monkey Striate Cortex (Area 17). *Cerebral Cortex*, *2*(4), 295–309. doi: 10.1093/cercor/2.4.295

Blundell, J., Blaiss, C. A., Etherton, M. R., Espinosa, F., Tabuchi, K., Walz, C., … Powell, C. M. (2010, feb). Neuroligin-1 Deletion Results in Impaired Spatial Memory and Increased Repetitive Behavior. *Journal of Neuroscience*, *30*(6), 2115–2129. doi: 10.1523/JNEUROSCI.4517-09.2010

Boström, K. J. (2013). Model for a flexible motor memory based on a self-active recurrent neural network. *Human Movement Science*, *32*, 880-898. doi: 10.1016/j.humov.2013.07.003

Bridi, M. C., Zong, F. J., Min, X., Luo, N., Tran, T., Qiu, J., ... Kirkwood, A. (2020, feb). Daily Oscillation of the Excitation-Inhibition Balance in Visual Cortical Circuits. *Neuron*, *105*(4), 621–629.e4. doi: 10.1016/J.NEURON.2019.11.011

Casanova, M. F., Buxhoeveden, D., & Gomez, J. (2003). Disruption in the Inhibitory Architecture of the Cell Minicolumn: Implications for Autisim. *Neuroscientist*, *9*(6), 496–507. doi: 10.1177/1073858403253552

Cazin, N., Llofriu Alonso, M., Scleidorovich Chiodi, P., Pelc, T., Harland, B., Weitzenfeld, A., ... Dominey, P. F. (2019, jul). Reservoir computing model of prefrontal cortex creates novel combinations of previous navigation sequences from hippocampal place-cell replay with spatial reward propagation. *PLoS Computational Biology*, *15*(7), e1006624. doi: 10.1371/journal.pcbi.1006624

Chen, J. L., Villa, K. L., Cha, J. W., So, P. T. C., Kubota, Y., & Nedivi, E. (2012). Clustered Dynamics of Inhibitory Synapses and Dendritic Spines in the Adult Neocortex. *Neuron*, *74*(2), 361–373. doi: 10.1016/j.neuron.2012.02.030

Chvatal, S. A., & Ting, L. H. (2012, aug). Voluntary and Reactive Recruitment of Locomotor Muscle Synergies during Perturbed Walking. *Journal of Neuroscience*, *32*(35), 12237–12250. doi: 10.1523/JNEUROSCI.6344-11.2012

Clark, D. J., Ting, L. H., Zajac, F. E., Neptune, R. R., & Kautz, S. A. (2010, feb). Merging of Healthy Motor Modules Predicts Reduced Locomotor Performance and Muscle Coordination Complexity Post-Stroke. *Journal of Neurophysiology*, *103*(2), 844–857. doi: 10.1152/jn.00825.2009

Delcomyn, F. (1980). Neural basis of rhythmic behavior in animals. *Science*, *210*(4469), 492–498. doi: 10.1126/science.7423199

Dichter, M., & Ayala, G. (1987, jul). Cellular mechanisms of epilepsy: a status report. *Science*, *237*(4811), 157–164. doi: 10.1126/science.3037700

Dominey, P. F. (2021, oct). Narrative event segmentation in the cortical reservoir. *PLOS Computational Biology*, *17*(10), e1008993. doi: 10.1371/journal.pcbi.1008993

Dominici, N., Ivanenko, Y. P., Cappellini, G., D'Avella, A., Mondì, V., Cicchese, M., ... Lacquaniti, F. (2011). Locomotor primitives in newborn babies and their development. *Science*, *334*(6058), 997–999. doi: 10.1126/science.1210617

Dudek, F. E., & Sutula, T. P. (2007). Epileptogenesis in the dentate gyrus: a critical perspective. In H. Scharfman (Ed.), *Progress in brain research* (Vol. 163, pp. 755–773). Elsevier. doi: 10.1016/S0079-6123(07)63041-6

Eccles, J. (1976). From Electrical to Chemical Transmission in the Central Nervous System. *Notes and Records of the Royal Society of London*, *30*(2), 219–230.

Enel, P., Procyk, E., Quilodran, R., & Dominey, P. F. (2016, jun). Reservoir Computing Properties of Neural Dynamics in Prefrontal Cortex. *PLOS Computational Biology*, *12*(6), e1004967. doi: 10.1371/journal.pcbi.1004967

Funahashi, K.-i., & Nakamura, Y. (1993, jan). Approximation of dynamical systems by continuous time recurrent neural networks. *Neural Networks*, *6*(6), 801–806. doi: 10.1016/S0893-6080(05)80125-X

Grillner, S. (1985, jan). Central Pattern Generators for Locomotion, with Special Reference to Vertebrates. *Annual Review of Neuroscience*, *8*(1), 233–261. doi: 10.1146/annurev.neuro.8.1.233

Hatze, H. (1980). A mathematical model for the computational determination of parameter values of anthropomorphic segments. *Journal of Biomechanics*, *13*(10), 833–843. doi: 10.1016/0021-9290(80)90171-2

Haykin, S. (2014). *Adaptive Filter Theory* (5th ed.). Upper Saddle River, NJ: Pearson.

Herstel, L. J., & Wierenga, C. J. (2021, apr). Network control through coordinated inhibition. *Current Opinion in Neurobiology*, *67*, 34–41. doi: 10.1016/j.conb.2020.08.001

Herzog, W. (1999). Muscle. In B. M. Nigg & W. Herzog (Eds.), *Biomechanics of the musculo-skeletal system*

(chap. Muscle). Wiley, Chichester.

Hinaut, X., & Dominey, P. F. (2013, feb). Real-Time Parallel Processing of Grammatical Structure in the Fronto-Striatal System: A Recurrent Network Simulation Study Using Reservoir Computing. *PLoS ONE*, *8*(2), e52946. doi: 10.1371/journal.pone.0052946

IJspeert, A. J. (2008, may). Central pattern generators for locomotion control in animals and robots: A review. *Neural Networks*, *21*(4), 642–653. doi: 10.1016/j.neunet.2008.03.014

Isaacson, J. S., & Scanziani, M. (2011, oct). How Inhibition Shapes Cortical Activity. *Neuron*, *72*(2), 231–243. doi: 10.1016/j.neuron.2011.09.027

Ivanenko, Y. P., Poppele, R. E., & Lacquaniti, F. (2004, apr). Five basic muscle activation patterns account for muscle activity during human locomotion. *The Journal of Physiology*, *556*(1), 267–282. doi: 10 .1113/jphysiol.2003.057174

Ivanenko, Y. P., Poppele, R. E., & Lacquaniti, F. (2006, feb). Spinal Cord Maps of Spatiotemporal Alpha-Motoneuron Activation in Humans Walking at Different Speeds. *Journal of Neurophysiology*, *95*(2), 602–618. doi: 10.1152/jn.00767.2005

Jaeger, H. (2010). *The "echo state" approach to analysing and training recurrent neural networks – with an Erratum note 1* (Tech. Rep. No. GMD 148). Hanover, Germany: German National Research Center for Information Technology.

Lacquaniti, F., Ivanenko, Y. P., & Zago, M. (2012, may). Patterned control of human locomotion. *J Physiol*, *590*(Pt 10), 2189–2199. doi: 10.1113/jphysiol.2011.215137

Lee, K. Y., Ratté, S., & Prescott, S. A. (2019). Excitatory neurons are more disinhibited than inhibitory neurons by chloride dysregulation in the spinal dorsal horn. *bioRxiv*, 1–23. doi: 10.1101/697417

Lukoševičius, M. (2012). A practical guide to applying echo state networks. *Lecture Notes in Computer Science*, *7700 LECTU*, 659–686. doi: 10.1007/978-3-642-35289-8-36

Maass, W., Natschläger, T., & Markram, H. (2002). Real-time computing without stable states: a new framework for neural computation based on perturbations. *Neural computation*, *14*(11), 2531–60. doi: 10.1162/089976602760407955

Marín, O. (2012). Interneuron dysfunction in psychiatric disorders. *Nature Reviews Neuroscience*, *13*(2), 107–120. doi: 10.1038/nrn3155

Markicevic, M., Fulcher, B. D., Lewis, C., Helmchen, F., Rudin, M., Zerbi, V., & Wenderoth, N. (2020, jul). Cortical Excitation:Inhibition Imbalance Causes Abnormal Brain Network Dynamics as Observed in Neurodevelopmental Disorders. *Cerebral Cortex*, *30*(9), 4922–4937. doi: 10.1093/cercor/bhaa084

Markram, H., Toledo-Rodriguez, M., Wang, Y., Gupta, A., Silberberg, G., & Wu, C. (2004). Interneurons of the neocortical inhibitory system. *Nature Reviews Neuroscience*, *5*(10), 793–807. doi: 10.1038/nrn1519

Marom, S., & Shahaf, G. (2002, feb). Development, learning and memory in large random networks of cortical neurons: lessons beyond anatomy. *Quarterly Reviews of Biophysics*, *35*(1), 63–87. doi: 10.1017/S0033583501003742

Megías, M., Emri, Z., Freund, T. F., & Gulyás, A. I. (2001). Total number and distribution of inhibitory and excitatory synapses on hippocampal CA1 pyramidal cells. *Neuroscience*, *102*(3), 527–540. doi: 10.1016/S0306-4522(00)00496-6

Meinecke, D. L., & Peters, A. (1987, jul). GABA immunoreactive neurons in rat visual cortex. *The Journal of Comparative Neurology*, *261*(3), 388–404. doi: 10.1002/cne.902610305

Murray, J. D., Anticevic, A., Gancsos, M., Ichinose, M., Corlett, P. R., Krystal, J. H., & Wang, X. J. (2014). Linking microcircuit dysfunction to cognitive impairment: Effects of disinhibition associated with schizophrenia in a cortical working memory model. *Cerebral Cortex*, *24*(4), 859–872. doi: 10.1093/cercor/bhs370

Neptune, R. R., Clark, D. J., & Kautz, S. A. (2009, jun). Modular control of human walking: A simulation

study. *Journal of Biomechanics*, *42*(9), 1282–1287. doi: 10.1016/j.jbiomech.2009.03.009

Okun, M., & Lampl, I. (2008, may). Instantaneous correlation of excitation and inhibition during ongoing and sensory-evoked activities. *Nature Neuroscience*, *11*(5), 535–537. doi: 10.1038/nn.2105

Okun, M., & Lampl, I. (2009). Balance of excitation and inhibition. *Scholarpedia*, *4*(8), 7467. doi: 10.4249/scholarpedia.7467

Peters, A. (2002). Examining neocortical circuits: Some background and facts. *Journal of Neurocytology*, *31*(3-5 SPEC. ISS.), 183–193. doi: 10.1023/A:1024157522651

Rajagopal, A., Dembia, C. L., DeMers, M. S., Delp, D. D., Hicks, J. L., & Delp, S. L. (2016, 09). Full-Body Musculoskeletal Model for Muscle-Driven Simulation of Human Gait. *IEEE Transactions on Biomedical Engineering*, *63*(10), 2068 – 2079. doi: 10.1109/tbme.2016.2586891

Rubenstein, J. L. R. (2010, apr). Three hypotheses for developmental defects that may underlie some forms of autism spectrum disorder. *Current Opinion in Neurology*, *23*(2), 118–123. doi: 10.1097/WCO.0b013e328336eb13

Rubenstein, J. L. R., & Merzenich, M. M. (2003, oct). Model of autism: increased ratio of excitation/inhibition in key neural systems. *Genes, Brain and Behavior*, *2*(5), 255–267. doi: 10.1034/j.1601-183X.2003.00037.x

Rubin, R., Abbott, L. F., & Sompolinsky, H. (2017, oct). Balanced excitation and inhibition are required for high-capacity, noise-robust neuronal selectivity. *Proceedings of the National Academy of Sciences*, *114*(44), E9366–E9375. doi: 10.1073/pnas.1705841114

Sahara, S., Yanagawa, Y., O'Leary, D. D. M., & Stevens, C. F. (2012, apr). The Fraction of Cortical GABAergic Neurons Is Constant from Near the Start of Cortical Neurogenesis to Adulthood. *Journal of Neuroscience*, *32*(14), 4755–4761. doi: 10.1523/JNEUROSCI.6412-11.2012

Selverston, A. I., Russell, D. F., Miller, J. P., & King, D. G. (1976). The stomatogastric nervous system: Structure and function of a small neural network. *Progress in Neurobiology*, *7*, 215–289. doi: https://doi.org/10.1016/0301-0082(76)90008-3

Shadlen, M. N., & Newsome, W. T. (1998). The variable discharge of cortical neurons: Implications for connectivity, computation, and information coding. *Journal of Neuroscience*, *18*(10), 3870–3896. doi: 10.1523/jneurosci.18-10-03870.1998

Shippen, J., & May, B. (2012). A kinematic approach to calculating ground reaction forces in dance. *Journal of dance medicine & science : official publication of the International Association for Dance Medicine & Science*, *16*(1), 39 – 43.

Sussillo, D., & Abbott, L. F. (2009). Generating Coherent Patterns of Activity from Chaotic Neural Networks. *Neuron*, *63*(4), 544–557. doi: 10.1016/j.neuron.2009.07.018

Tabuchi, K., Blundell, J., Etherton, M. R., Hammer, R. E., Liu, X., Powell, C. M., & Südhof, T. C. (2007, oct). A Neuroligin-3 Mutation Implicated in Autism Increases Inhibitory Synaptic Transmission in Mice. *Science*, *318*(5847), 71–76. doi: 10.1126/science.1146221

Tatti, R., Swanson, O. K., Lee, M. S., & Maffei, A. (2017, nov). Layer-specific Developmental Changes in Excitation and Inhibition in Rat Primary Visual Cortex. *eNeuro*, *4*(6). doi: 10.1523/ENEURO.0402-17.2017

Thaller, S., & Wagner, H. (2004). The relation between hill's equation and individual muscle properties. *Journal of Theoretical Biology*, *231*(3). doi: 10.1016/j.jtbi.2004.06.027

Todd, A. J., & Sullivan, A. C. (1990, jun). Light microscope study of the coexistence of GABA-like and glycine-like immunoreactivities in the spinal cord of the rat. *The Journal of Comparative Neurology*, *296*(3), 496–505. doi: 10.1002/cne.902960312

Tsodyks, M. V., & Sejnowski, T. (1995, jan). Rapid state switching in balanced cortical network models. *Network: Computation in Neural Systems*, *6*(2), 111–124. doi: 10.1088/0954-898X_6_2_001

Van Vreeswijk, C., & Sompolinsky, H. (1996, dec). Chaos in Neuronal Networks with Balanced Excitatory

and Inhibitory Activity. *Science*, *274*(5293), 1724–1726. doi: 10.1126/science.274.5293.1724

van Vreeswijk, C., & Sompolinsky, H. (1998, aug). Chaotic Balanced State in a Model of Cortical Circuits. *Neural Computation*, *10*(6), 1321–1371. doi: 10.1162/089976698300017214

Verstraeten, D., Schrauwen, B., D'Haene, M., & Stroobandt, D. (2007). An experimental unification of reservoir computing methods. *Neural Networks*, *20*(3), 391–403. doi: 10.1016/j.neunet.2007.04.003

Wehr, M., & Zador, A. M. (2003, nov). Balanced inhibition underlies tuning and sharpens spike timing in auditory cortex. *Nature*, *426*(6965), 442–446. doi: 10.1038/nature02116

Winter, D. A. (2009). *Biomechanics and Motor Control of Human Movement*. Hoboken, NJ, USA: John Wiley & Sons, Inc. doi: 10.1002/9780470549148

Wonders, C. P., & Anderson, S. A. (2006). The origin and specification of cortical interneurons. *Nature Reviews Neuroscience*, *7*(9), 687–696. doi: 10.1038/nrn1954

Wyffels, F., & Schrauwen, B. (2009). Design of a central pattern generator using reservoir computing for learning human motion. *Proceedings - 2009 Advanced Technologies for Enhanced Quality of Life, AT-EQUAL 2009*, 118–122. doi: 10.1109/AT-EQUAL.2009.32

Yaksh, T. L. (1989, apr). Behavioral and autonomic correlates of the tactile evoked allodynia produced by spinal glycine inhibition: effects of modulatory receptor systems and excitatory amino acid antagonists. *Pain*, *37*(1), 111–123. doi: 10.1016/0304-3959(89)90160-7

Yizhar, O., Fenno, L. E., Prigge, M., Schneider, F., Davidson, T. J., O'Shea, D. J., ... Deisseroth, K. (2011, sep). Neocortical excitation/inhibition balance in information processing and social dysfunction. *Nature*, *477*(7363), 171–178. doi: 10.1038/nature10360

Zhou, S., & Yu, Y. (2018, feb). Synaptic E-I Balance Underlies Efficient Neural Coding. *Frontiers in Neuroscience*, *12*(FEB), 1–11. doi: 10.3389/fnins.2018.00046

Appendix A Calculation of spinal cord efferent and afferent signals using computational musculo-skeletal model Myonardo

Myonardo is a Matlab-based, 3D computational musculo-skeletal model, that consists of 17 bone segments, 19 joints and 180 muscle-tendon-units. For the present study 8 of these muscle-tendon-units were analyzed: *m. flexor hallucis longus*, *m. gastrocenemius*, *m. gluteus maximus*, *m. gluteus medius*, *m. gluteus minimus*, *m. piriformis*, *m. semitendinosus*, and *m. tensor fasciae latae*. The relative mass and size of the individual segments, as well as the muscular attachments were determined based on the work of Shippen & May (2012). The entire model was scaled to the subject's body mass and height (Winter, 2009; Hatze, 1980).

As a first step, *Myonardo* calculated the muscle-tendon lengths, muscle-tendon velocities and the muscular lever arms relative to the instantaneous joint center, based on the instantaneous joint angles and joint angular velocities acquired from the 3D kinematics. The muscle line of action between the origin and the insertion of each muscle-tendon unit is separated into muscle parts between via-points, such that the muscle length was calculated as the sum of the length of each muscle part, i.e. the euclidean distance between the attachments of the muscle part.

Based on these muscle lengths l_m and velocities v_m, the maximum possible muscle force $f_{m,max}$, could then be calculated using the force-velocity relation (f_v), as well as the active (f_{la}) and passive (f_{lp}) force-length relations as follows:

$$f_{m,max} = Act(t) \cdot f_v \cdot f_{la} + f_{lp} \tag{6}$$

where $Act(t)$ - the activation of the muscle in the interval [0,1] - was set to 1. The Hill-type force-velocity relation (f_v) was calculated as:

$$f_v(v_m) = \begin{cases} \frac{c}{v_m+b} - a & \text{if } v_m \leq 0 \\ \frac{C}{v_m-B} + A & \text{if } v_m > 0 \end{cases} \tag{7}$$

where properties a, b, c and A, B, C were estimated from the isometric force f_{iso}, resting length l_{opt}, eccentric gain f_{ecc} and the ratio of fast-twitch to slow-twitch fibres $FT\%$, using parameter values from (Thaller & Wagner, 2004) and (Herzog, 1999). The active ($f_l a$) and passive ($f_l p$) force-length relations

were calculated as:

$$f_{la}(l_m) = exp\left[-(\frac{(l_m/l_{opt})^{k_1}-1}{k_2})^{k_3}\right] \tag{8}$$

$$f_{lp}(l_m) = exp((l_m - l_{opt})/k_4) \tag{9}$$

with $k_1 = 0.96$, $k_2 = 0.35$, $k_3 = 2$, $f_{ecc} = 1.5$, and $FT\% = 0.5$. The remaining muscle properties f_{iso} and l_{opt} were taken from Rajagopal et al. (2016).

Based on the maximum force $f_{m,max}$ for each muscle and the lever arms r, the maximum force that each muscle can generate around a joint at a certain instance of time was calculated as $T_{max} = r \times f_{m,max}$. Then a set of muscular activations $Act(t)$, within the boundary $0 \leq Act \leq 1$, can be determined for each joint, such that

$$T_{net} = \sum_{i=1}^{n} T_{max_i} \cdot Act_i \tag{10}$$

with i indicating the n muscles that are acting at the given joint. The required net torque T_{net} is known from inverse dynamics and the maximum torque T_{max} was calculated as described above. As there are more muscles than degrees of freedom of a joint contributing to the joint-torques, the muscular activation of these redundant muscles have to be distributed via optimization. In the present study, the muscular activation was calculated by minimizing the sum of squared muscular activations for each instant of time based on the linear least-squares solver (`lsqlin`):

$$\min_{Act} \| Act \|^2 \tag{11}$$

Appendix B FORCE learning algorithm

To train the network, we used the FORCE algorithm (Sussillo & Abbott, 2009), which is based on a recursive least squares approach (Haykin, 2014)

The output signals were calculated by multiplying the $[k \times N]$-dimensional output weights matrix $\boldsymbol{W}(t)$ with the sigmoid-transformed neuron activations $\boldsymbol{r}(t) = \begin{bmatrix} r_{ij}^E & r_{ij}^I \end{bmatrix}$.

$$\boldsymbol{Y}(t) = \boldsymbol{W}(t) \cdot \boldsymbol{r}(t) \tag{12}$$

The output error $\boldsymbol{\epsilon}$ (k-dimensional row vector) was calculated as the difference between the calcu-

lated output $\boldsymbol{Y}(t)$ and the target output $\boldsymbol{Y_{target}}(t)$.

$$\boldsymbol{\epsilon}(t) = \boldsymbol{Y}(t) - \boldsymbol{Y}_{target}(t) \tag{13}$$

The output weights $\boldsymbol{W}(t)$ were updated based on the current activity, the output error $\boldsymbol{\epsilon}$, and the learning rate matrix $\boldsymbol{P}(t)$ ([NxN] matrix). $\boldsymbol{P}(t)$ denotes an estimate of the inverse of the correlation matrix of $\boldsymbol{r}(t)$ with a regularization term Sussillo & Abbott (2009).

$$\boldsymbol{W}(t+\Delta t) = \boldsymbol{W}(t) - \epsilon(t)\frac{\boldsymbol{P}(t)\boldsymbol{r}(t)}{1+\boldsymbol{r}(t)^T\boldsymbol{P}(t)\boldsymbol{r}(t)} \tag{14}$$

$\boldsymbol{P}(t)$ was updated according to the equation below.

$$\boldsymbol{P}(t+\Delta t) = \boldsymbol{P}(t) - \frac{\boldsymbol{P}(t)\boldsymbol{r}(t)\cdot(\boldsymbol{P}(t)\boldsymbol{r}(t))^T}{1+\boldsymbol{r}(t)^T\boldsymbol{P}(t)\boldsymbol{r}(t)} \tag{15}$$

Appendix C Supplementary Figures

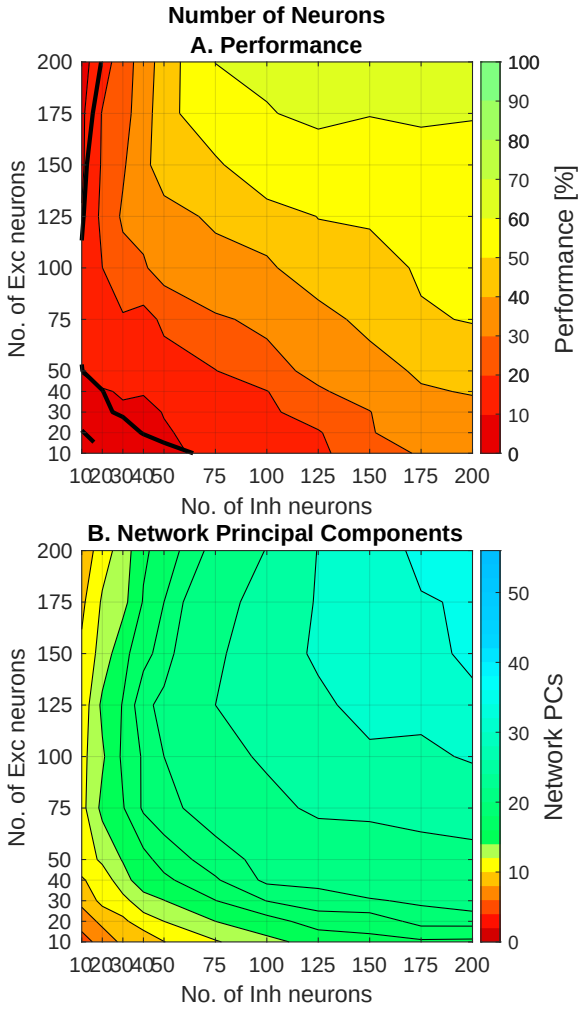

Figure S.1 – Influence of neuron number in small networks on network performance and internal network dynamics *(A-E.) Network performance and (B-J.) Network Principal Components. The thick, dashed-dotted lines in both panels represent the contour lines for 11 network principles components, corresponding to the number of components needed to explain 99% of variance in the target output. This is a zoomed in version of Figure 1A&D.*

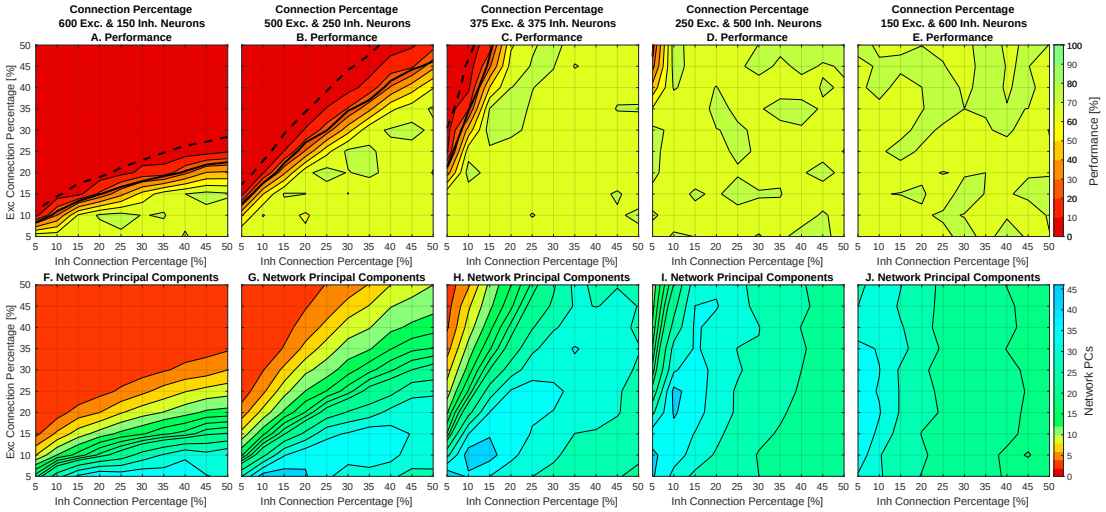

Figure S.2 – Influence of connection percentage on network performance and internal network dynamics *(A-E.) Network performance and (B-J.) Network Principal Components for five different ratios of excitatory to inhibitory neuron numbers. The thick, dashed-dotted lines in all panels represent the contour lines for 11 network principles components, corresponding to the number of components needed to explain 99% of variance in the target output.*

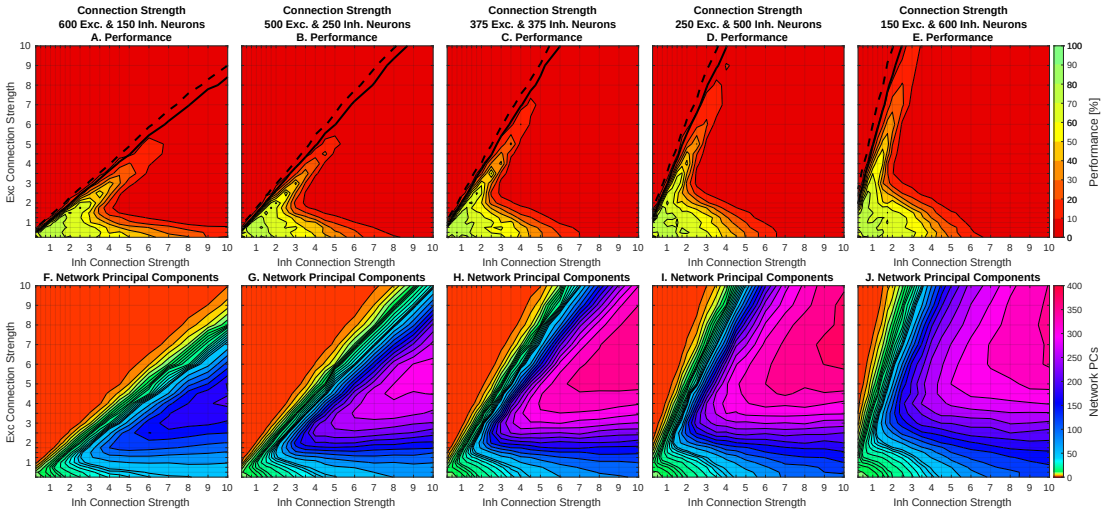

Figure S.3 – Influence of connection strength on network performance and internal network dynamics *(A-E.) Network performance and (B-J.) Network Principal Components for five different ratios of excitatory to inhibitory neuron numbers. The thick, dashed-dotted lines in all panels represent the contour lines for 11 network principles components, corresponding to the number of components needed to explain 99% of variance in the target output.*

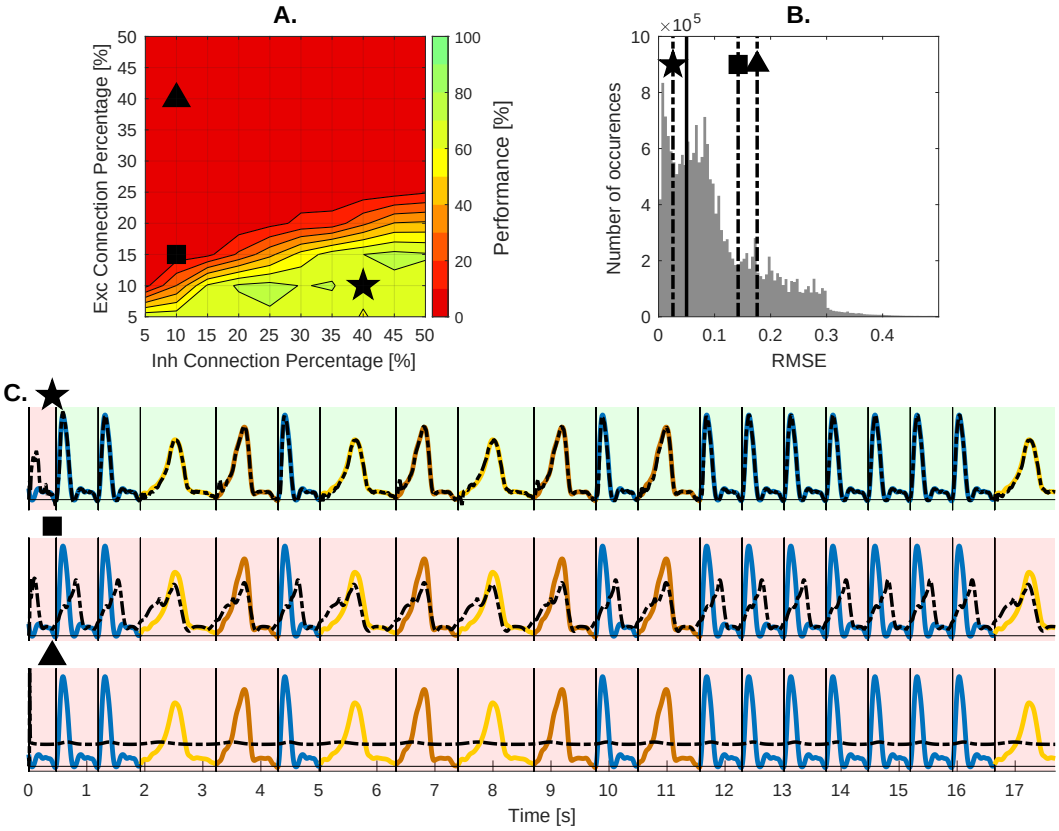

Figure S.4 – Reduction in motor variability for excitatory imbalance. ***(A.)*** *Performance of networks with varying connection percentage,* $N_E = 600, N_I = 150$*, and* $g_E = g_I = 150$*.* ***(B.)*** *Distribution of the RMSE per gait cycle over all tested networks.* ***(C.)*** *Example motor output for three example networks; top row (star): network imbalanced towards inhibition with good performance; middle row (square): network slightly imbalanced towards excitation with reduced motor variability; bottom row (triangle): network highly imbalanced towards excitation with almost no motor variability. The connection percentages and RMSEs of the three example networks are indicated in panels (**A**) and (**B**) as a star, a square and a triangle.*